

Improved Ultrahigh-Resolution Wind Retrieval for RapidScat

Nolan Hutchings and David G. Long^{ID}, *Fellow, IEEE*

Abstract—This paper introduces RapidScat 2.5-km ultrahigh-resolution (UHR) wind estimation and validates it in near-coastal regions. RapidScat UHR wind estimation provides finer resolution ocean wind vector fields than conventional 12.5-km level 2B (L2B) wind products at a cost of higher noise. In addition, this paper applies direction interval retrieval techniques and develops other wind processing improvements to enhance the performance of RapidScat UHR wind estimation. The new algorithm is validated with L2B wind estimates, numerical weather prediction wind products, and buoy measurements. The wind processing improvements produce more spatially consistent UHR winds that compare well with the wind products mentioned above.

Index Terms—Radar scattering, RapidScat, scatterometer, wind.

I. INTRODUCTION

SCATTEROMETERS are active microwave sensors that estimate wind speed and direction over the open ocean by measuring the normalized radar cross section (σ^0) from a wind-roughened ocean surface. Wind vector data from scatterometers are used in a variety of oceanic studies and in weather forecasting [1], [2]. RapidScat is a dual pencil-beam Ku-band (13.4 GHz) scatterometer that operated on the International Space Station (ISS) from October 2014 to August 2016 [3]. RapidScat's σ^0 measurements are used to produce a coarse 12.5-km resolution grid of wind vector (speed and direction) estimates [referred to as level 2B (L2B) [4]], which have been validated with numerical weather prediction (NWP) winds and buoy measurements [3], [5], [6]. Each resolution element in the grid is called a wind vector cell (WVC).

To enable wind retrieval over the ocean, σ^0 measurements are collected at multiple azimuth/incidence angles (“looks”) at each WVC in the coverage swath. Wind retrieval requires diverse σ^0 measurements to solve for both wind speed and direction. RapidScat obtains multiple look angles via its rotating dual-beam antenna, which provides multiple azimuth angles and up to two different incidence angles for each WVC. This results in up to four categories of backscatter measurements (sometimes called “flavors”) for each WVC where

measurements within each category have similar azimuth and incidence angles but the categories have a different azimuth and/or incidence angle [4].

RapidScat wind retrieval uses a geophysical model function (GMF) to relate the σ^0 measurements in each WVC to 10-m equivalent neutral wind vectors [7]. A likelihood objective function, $f(u, \phi)$, is formulated for the wind speed (u) and direction (ϕ) of a particular WVC using the measured σ^0 (σ_{0i}), noise variance parameters (sd_i) [8], and the GMF evaluated at $u, \phi, (\sigma'_{0i})$

$$f(u, \phi) = - \sum_i \left(\frac{\sigma_{0i} - \sigma'_{0i}(u, \phi)}{sd_i} \right)^2. \quad (1)$$

The multiple local maxima of the objective function lead to several possible solutions [9].

Each wind speed and direction pair associated with the objective function's local maxima is referred to as an “ambiguity.” There are up to four ambiguities for each WVC. The ambiguities have similar wind speeds, but different wind directions [4]. Selection of a unique estimate, a process called “ambiguity selection,” begins by creating an initial wind field of estimates by “nudging” the grid of ambiguous solutions with another wind product (e.g., NWP winds for RapidScat L2B), which is referred to as the “nudging field.” For each WVC in the swath, the nudging process selects the ambiguity that is closest in direction to the corresponding wind from the nudging field [8]. The resulting wind field is referred to as the “nudged field.”

The nudged wind field is then iteratively updated using a median filter-based ambiguity selection scheme (MAS) to produce a more spatially consistent final wind vector field [8], [10], [11]. For each WVC, the MAS compares the directions of its ambiguities with the directions of the selected ambiguities of the surrounding WVCs contained in the filter window. The ambiguity of the center WVC that is the direction closest to the circular median direction of the window is chosen to replace the current ambiguity choice for the center WVC. The MAS iterates until a passthrough in the whole swath is completed without any ambiguity choices being changed or until the maximum number of iterations (100) is reached [10].

Ambiguity selection in scatterometer wind processing has historically proven to be difficult and prone to error. Ambiguity selection is especially difficult in the nadir and far-swath regions for pencil-beam scatterometers [8]. Due to a limited azimuth angle diversity in these regions, the wind retrieval

Manuscript received June 15, 2018; revised September 29, 2018 and November 21, 2018; accepted November 25, 2018. Date of publication December 21, 2018; date of current version May 28, 2019. (Corresponding author: David G. Long.)

The authors are with the Electrical and Computer Engineering Department, Brigham Young University, Provo, UT 84602 USA (e-mail: long@ee.byu.edu).

Color versions of one or more of the figures in this paper are available online at <http://ieeexplore.ieee.org>.

Digital Object Identifier 10.1109/TGRS.2018.2884128

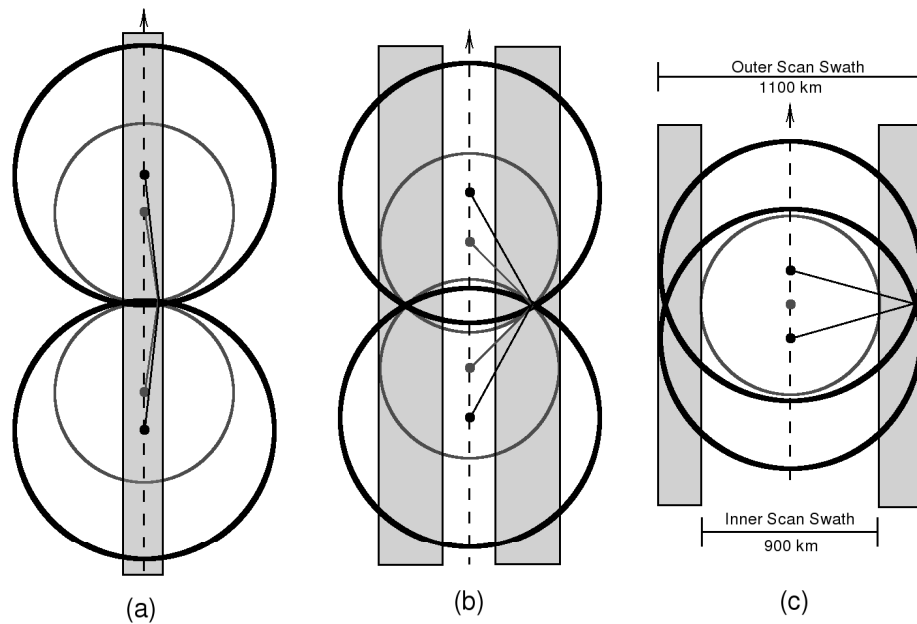


Fig. 1. Illustrations of beam orientations for (a) nadir, (b) “sweet spot,” and (c) far-swath looks. Dashed lines: nadir satellite path. The bold dots along the dashed lines are satellite positions in the swath at different times. The lines extending from the dots show the azimuth angles of the beams for a particular WVC. Smaller circles: inner beam’s reach. Larger circles: outer beam’s reach. The shaded boxes contain WVCs that have similar quality azimuth looks as the ones depicted. Note that for (a), there are effectively only two azimuth angles, while for (c), there is effectively only a single azimuth angle. In (b), there are four azimuth angles.

process can generate inaccurate solutions for ambiguity selection. In particular, the azimuth angles of fore and aft looks in the nadir region are almost 180° apart [see Fig. 1(a)]. In the far-swath region, there are only measurements from the outer beam, and they have similar azimuth angles [see Fig. 1(c)]. For comparison, Fig. 1(b) shows the beam orientations of optimal “sweet spot” looks. Adverse weather conditions can also result in poor wind retrieval (e.g., rain).

We note that RapidScat’s mounting on the ISS presents some complications for wind estimation. For antenna azimuth angles 70° – 116° , the RapidScat transmitter does not emit in order to avoid exposing docked spacecraft to the transmitted signal [3]. This gap in emission is referred to as “sector blanking.” Sector blanking produces fewer σ^0 measurements in bands of WVCs, which adversely affects wind estimation accuracy. Sector blanking can also result in data gaps in the estimated wind field swath. Another complication is that wind estimation can fail in near-coastal regions due to land contamination of ocean σ^0 measurements. Land contamination refers to the effects of the higher reflectivity of the land in comparison to the water. Antenna side lobes can allow strong land echoes to “contaminate” the lower ocean σ^0 measurements, which leads to erroneous wind speed values in near-coastal regions. Previously, land contamination was avoided by discarding wind estimates that fall within 30 km of land. However, wind estimates closer to the coast can be retrieved with the spatial response function (SRF) and a binary land map, which are used to calculate the land contamination ratio (LCR) [12]. For each σ^0 measurement, an LCR is computed and thresholded to decide if the σ^0 measurement is contaminated by land. Using only uncontaminated

σ^0 measurements enables accurate wind retrieval much closer to land [12].

To further advance wind estimation in near-coastal regions, in this paper we produce RapidScat wind estimates on an ultrahigh-resolution (UHR) 2.5-km WVC grid. Instead of directly using “egg” or “slice” σ^0 measurements as in L2B wind retrieval [13], UHR processing applies reconstruction techniques to enhance spatial resolution of the σ^0 values prior to wind retrieval [14]. UHR wind processing reveals finer resolution detail of ocean wind phenomena and, with LCR applied in near-coastal regions, allows for wind vector estimates even closer to shore than is possible with L2B estimates.

With the higher resolution of UHR comes added noise in the estimates. UHR wind estimates also suffer from the same wind retrieval and ambiguity selection problems as L2B wind estimates. Direction interval retrieval (DIR) has been developed to improve ambiguity selection accuracy in the nadir and far swath for QuikSCAT L2B winds [8]. In this paper, the method is applied to RapidScat UHR wind estimation. Other methods such as artificial ambiguities (AAs) are introduced and validated. These methods improve UHR wind estimation accuracy. The results are validated with moored buoy data and L2B wind estimates.

This paper is organized as follows. Section II describes RapidScat UHR processing and the validation process for near-coastal estimates. Section III outlines the MAS for RapidScat UHR estimates. Section IV discusses the application of DIR to RapidScat UHR wind estimates. In Section V, improved wind retrieval and ambiguity selection methods for RapidScat UHR estimates are introduced. The remaining

Sections VI and VII report the results of the validation and the conclusions reached.

II. UHR WIND ESTIMATION

UHR wind estimation is not unique to RapidScat and has previously been applied in ASCAT and QuikSCAT wind estimation [12], [15], [16]. Each sensor has a different approach to wind retrieval but has the same approach in generating UHR σ^0 . Low resolution σ^0 and the sensor's SRF are used to produce UHR σ^0 fields. UHR wind estimates are generated from the UHR σ^0 using the same wind processing procedure that is performed on low-resolution estimates, including the same GMF and objective function. As described earlier, UHR estimates can potentially estimate wind features closer to shore and also reveal finer resolution wind phenomena. We choose to validate RapidScat UHR estimates in a near-coastal region off the East Coast of the United States due to a large number of buoys available for collocation. In addition, RapidScat UHR estimates are compared with L2B estimates.

A. Validation of Near-Coastal UHR Wind Estimates

Near-coastal RapidScat UHR wind estimates with LCR are validated by collocating UHR wind vectors with offshore buoy measurements and L2B estimates. A collocated UHR estimate is the UHR wind vector located closest to the buoy (within 2.5 km) and collected within 30 min of the buoy measurement. L2B collocations are within 12.5 km and 30 min of the buoy measurement. Buoy data are taken from the National Data Buoy Center (NDBC) [17]. Because of varying anemometer heights among the buoys, the buoy measurements are converted to represent 10-m equivalent neutral wind vectors to match the reported scatterometer data [7]. Buoy data provide an 8-min temporally averaged measurement of wind speed and direction.

UHR estimates are averaged over a 5×5 WVC window (same area as a single L2B WVC) around the center collocated UHR WVC for comparison with the low-resolution L2B estimates. The same averaging approach is used for comparison with buoy measurements. The UHR ambiguities averaged in the window are the ambiguities of each WVC with the direction closest to the reported buoy direction (this choice of ambiguity is referred to as C2B, closest to buoy). The C2B ambiguity represents the best case scenario for the ambiguity selection.

The buoys used in this paper are located on the southeast coast of the United States (see Fig. 2) and satisfy the same criteria as in [18]: only moored sea buoys that have data necessary for U10 conversion, air and sea surface temperatures, surface pressure, and near-surface relative humidity, are used. Buoy measurements are treated as “true” values in this paper. For more regarding buoy-based validation, refer to [18].

A year's worth of RapidScat wind estimates, taken from August 2015 through August 2016, is collocated with buoys. A total of 4856 buoy collocations are found in the study region shown in Fig. 2. We note that in August 2015, RapidScat experienced a 10-dB increase in noise [3]. The increase in noise level was not constant and varied between low- and

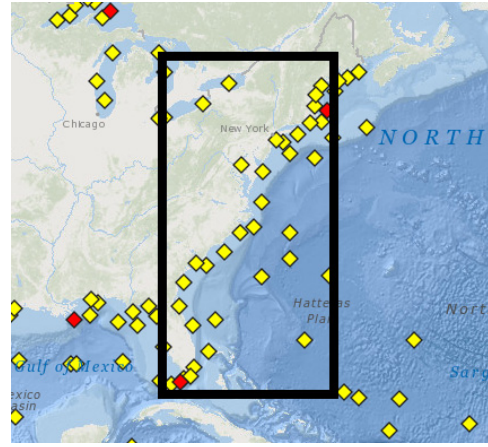


Fig. 2. Buoy locations from NDBC and the approximate region used in this paper. Latitude 25 to 45 N and Longitude 82 to 70 W. Figure modified from [17].

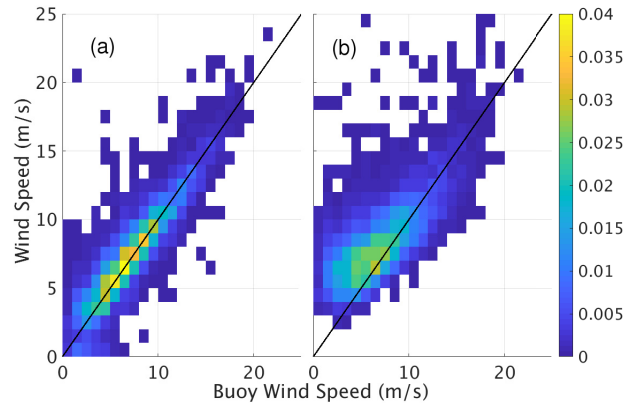


Fig. 3. Scatter density plots of (a) L2B and (b) UHRB wind speeds plotted with collocated buoy wind speed measurements. A $y = x$ (solid line) line is included for reference. UHRB wind speed estimates are noisier and biased higher, especially at low wind speeds.

high-noise states. The high-noise state was prevalent for most of the mission after the problem arose. The increase in noise results in degraded wind speed estimation. Of the original 1154 orbits in which collocations occur, 81 are deemed poor or marginal quality due to high noise and are subsequently removed from the study, resulting in the number of collocations stated earlier. Section II-A1 discusses the wind speed comparison between C2B UHR (hereafter referred to as UHRB), L2B, and buoy measurements. Section II-A2 is an analysis of the UHRB wind direction.

1) *UHRB Wind Speed Accuracy*: We first consider wind speed. In Fig. 3, L2B (a) and UHRB (b) wind speed estimates are plotted against buoy wind speed measurements. The plots reveal that the L2B estimates match the buoys over a wide range of wind speeds. However, UHR processing overestimates low wind speeds and the UHRB estimates are noisier than the L2B wind vectors for most wind speeds. For moderate wind speeds (7–15 m/s), UHRB has similar results as that of the L2B wind speed estimates. Due to the limited number of observations, it is difficult to draw conclusions on high wind speed estimates.

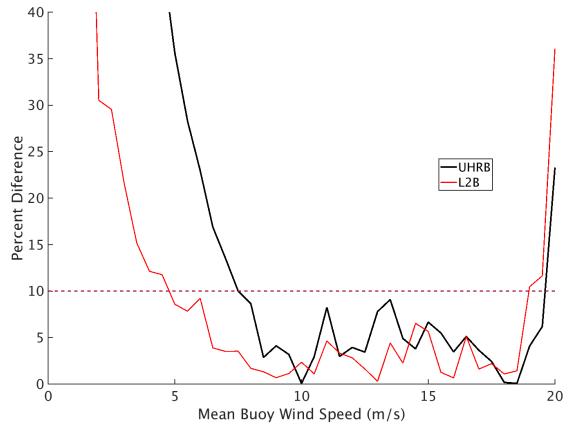


Fig. 4. Percentage difference of mean L2B and mean UHRB estimates from mean buoy measurements. Horizontal dashed line: 10% difference boundary. Mean UHRB estimates exceed the boundary below 7 m/s, while mean L2B exceeds the boundary below 5 m/s. There are too few measurements at high wind speeds to draw any conclusions.

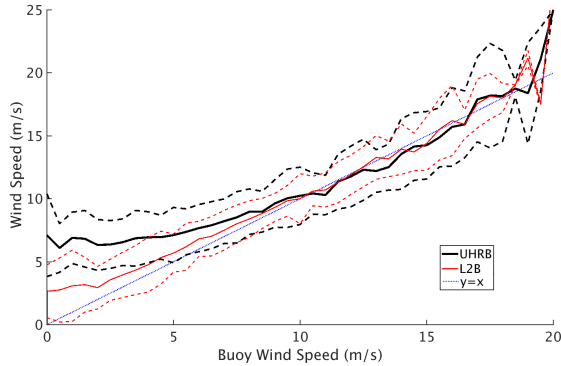


Fig. 5. Plot of mean UHRB and L2B wind speeds (solid) with standard deviation (dashed) lines versus buoy wind speed. A $y = x$ line is included for reference.

In Fig. 4, the collocated UHRB and L2B wind speeds are averaged within 0.5-m/s buoy wind speed bins and the percentage difference from the mean buoy wind speeds is shown. Consistent with Fig. 3, at low wind speeds, the UHRB estimates exhibit greater difference than L2B compared to the buoy measurements. The plot shows that for wind speeds over 7 m/s and below 18 m/s, the UHRB estimates are on average within 10% of buoy measurements. This is within the accepted accuracy requirements given in [18], i.e., that estimates are within 10% or 1 m/s of buoy measurements. Fig. 5 presents a comparison of mean UHRB and L2B wind speeds with standard deviation lines. Remarkably, the standard deviation for both UHRB and L2B is similar for all wind speeds. However, for low wind speeds, the UHRB estimates are biased high, which is consistent with higher noise in the estimates [18]. The plot shows the same trends for low, middle, and high wind speeds as the previously mentioned plots.

2) *UHRB Wind Direction Accuracy*: Wind directions are now considered. Fig. 6 presents L2B (a)–(c) and UHRB (d)–(f) wind directions with collocated buoy measurements sorted by wind speed. The top row has collocations

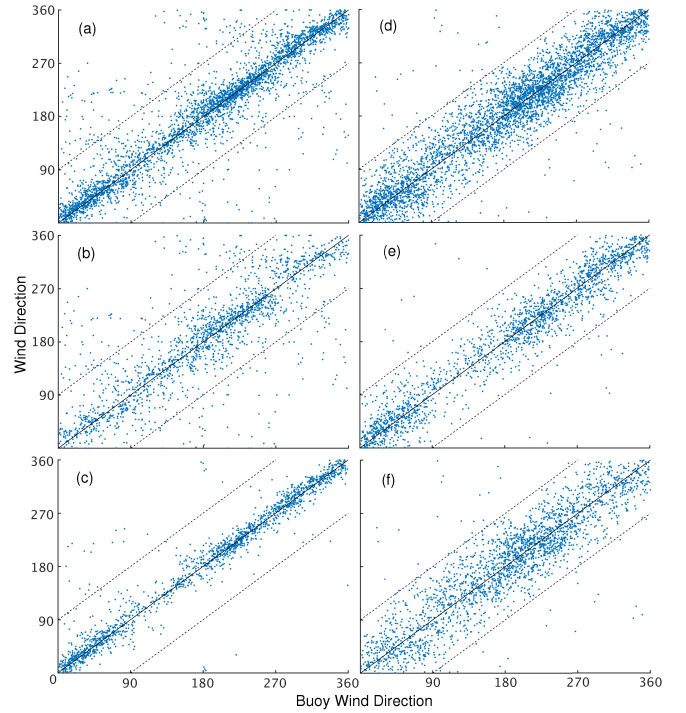


Fig. 6. Plots of (a)–(c) RapidScat L2B and (d)–(f) UHRB wind directions with collocated buoy measurements sorted by wind speed. (Top row) Collocations for all the wind speeds. (Middle row) Collocations with wind speeds below 7 m/s. (Bottom row) Collocations with wind speeds above 7 m/s. Dashed lines: $\pm 90^\circ$ from the ideal $y = x$ line. Due to the circular nature of direction values, for clarity in plotting, we wrapped the points in the corners $x < 90^\circ$, $y > 270^\circ$ by subtracting 360° and $x > 270^\circ$, $y < 90^\circ$ by adding 360° .

at all wind speeds, the middle row at wind speeds less than 7 m/s, and the bottom row at wind speeds greater than 7 m/s. As expected, the UHRB wind direction estimates are noisier than the L2B winds. However, the UHRB direction estimates tend to be more concentrated within $\pm 90^\circ$ than the L2B winds at low wind speeds. Fig. 7 shows the L2B and UHRB circular mean and standard deviation of the angular difference from buoy measurements. Due to the circular nature of the direction angles, a circular mean is computed, which is done as the four-quadrant inverse tangent of the sum of the sine and cosine of the directions, that is,

$$\mu_c = \text{atan2} \left\{ \sum_{i=1}^n \sin(\theta_i), \sum_{i=1}^n \cos(\theta_i) \right\} \quad (2)$$

where μ_c is the circular mean, n is the number of directions in a given bin, and θ_i is the direction of the i th value. The circular means of both L2B and UHRB are consistent, i.e., they both closely follow the $y = x$ line. Furthermore, the standard deviation of the UHRB estimates is similar to that of the L2B estimates. The observed variation in standard deviation with the buoy direction that appears in both the UHRB and L2B winds is puzzling but may be related to the look of the backscatter measurements in wind retrieval.

3) *Summary of Near-Coastal UHRB Performance*: Based on buoy comparisons, UHRB wind vectors are generally reliable despite being noisier than L2B estimates. At low

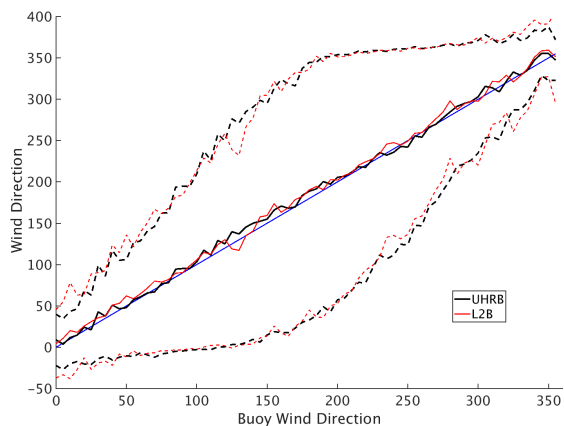


Fig. 7. Comparison of UHRB and L2B circular mean directions (solid lines) with collocated mean buoy measurements. Dashed lines: one standard deviation of the angular difference from buoy measurements, see text.

wind speeds (<7 m/s), the UHRB estimates are biased high. At higher wind speeds, UHRB wind speed estimates better match the buoy measurements than at lower speeds.

UHRB direction estimates are not as tightly grouped around the $y = x$ line as the L2B direction estimates, confirming they are noisier. However, the UHRB winds tend to be within $\pm 90^\circ$ more than L2B estimates for lower wind speeds. We emphasize that UHRB represents the best case ambiguity selection scenario, in that it has “perfect” ambiguity selection with respect to the buoy directions. Nevertheless, the results demonstrate the potential of RapidScat UHR wind estimates in near-coastal regions. We note that the L2B estimates used in the comparison use the ambiguity provided by the NASA Jet Propulsion Laboratory that may not have “perfect” ambiguity selection. In Section VI, the performance of the ambiguity selected wind is compared to buoy measurements.

III. MAS

As previously noted, the MAS is used to select a unique ambiguity at each WVC [10]. The MAS can smooth out the nudged wind fields while still preserving wind fronts [19]. The window size is an important consideration when designing the filter [11]. A variety of window sizes, ranging from 17.5–77.5 km, were tested for RapidScat UHR ambiguity selection. If the window is too small, inconsistencies can overwhelm the filter and result in large areas of inconsistent ambiguity choices. This generally occurs only in the nadir and far swath. A window that is too small can also be blind to larger wind features. Excessively large filters are computationally taxing and have diminishing returns as far as improved accuracy is concerned. Another consideration is the root-mean-square (rms) difference from NWP winds. A comparison of the rms difference from NWP wind directions for different median filter window sizes compared to L2B rms differences is shown in Fig. 8. Fig. 8 shows that rms difference decreases as filter size increases. Based on this analysis, a window size of 52.5 km is chosen (dashed line in Fig. 8). This corresponds to a 21×21 UHR WVC window. The 52.5-km window preserves both large and small wind features,

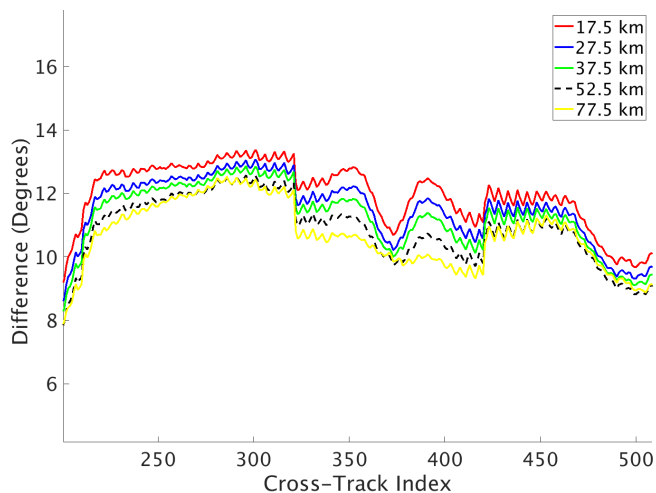


Fig. 8. Difference between the rms of the difference of UHR and NWP winds and the rms of the difference of L2B and NWP winds for different median filter window sizes for UHR ambiguity selection.

lowers rms difference, and has an acceptable computational burden.

IV. DIR

DIR, while originally developed for conventional L2B data, can be applied to UHR wind retrieval to improve the wind estimates. A brief description of DIR is provided in this section. Another previously developed algorithm, thresholded nudging (TN), is briefly considered for RapidScat application at the end of this section.

DIR was developed to improve wind estimation accuracy for QuikSCAT L2B estimates in the nadir region [8]. In this paper, the nadir region is defined to be within 125 km of the nadir track. As previously noted, the nadir region lacks the azimuth angle diversity required for accurate wind direction determination because the σ^0 measurement angles are close to 180° apart (see Fig. 1). The lack of azimuth diversity results in regions around the objective function’s local maxima that are close to the value of the local maxima themselves (see Fig. 9). Typical of this problem, the objective function has a “wide” local maxima that incorporates a range of wind vectors that yield similar objective function values. When this happens, the most spatially consistent wind estimate may not be associated with the objective function maximum but may be nearby with a similar objective function value. This wide maxima effect is not specific to the nadir region but is most commonly seen there.

Rather than reporting a single direction value for each ambiguity as in conventional wind retrieval, DIR captures the range of wind direction solutions that are similar in likelihood to the local maxima. The range of solutions is then used in a modified MAS that selects a spatially consistent value from within the range of solutions. Fortunately, there is little variation in wind speed around the area of the local maxima, so the wind speed assumed for the range of directions is the wind speed associated with its respective maximum.

Our implementation of DIR is performed by determining a range of directions around each local maximum. The range is

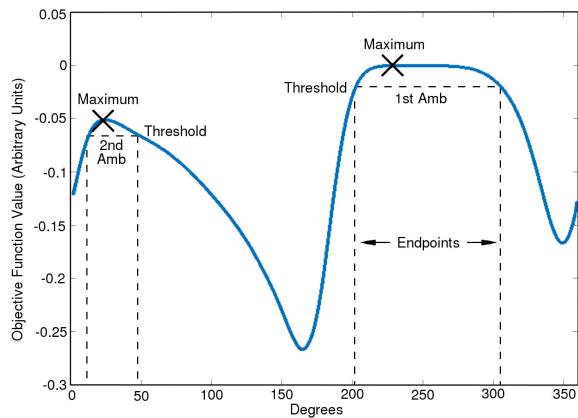


Fig. 9. Example objective function with two local maxima, arbitrarily placed thresholds, and the resulting endpoint boundaries (the vertical dashed lines).

defined by a boundary to either side of the local maximum. The endpoints of the boundary are found by taking a fraction of the value of the objective function at each local maximum to create a threshold (see Fig. 9). The fraction 0.2 was subjectively chosen; however, the DIR algorithm is relatively insensitive to the precise fraction value. This value is adjusted to ensure a minimum of 30° between the endpoints. This use of minimum range differs from that in [8].

To compute the DIR range, the routine iterates along the objective function at 1.0° steps on either side of the local maximum until the threshold is reached. When the objective function reaches the threshold on either side, the respective directions are used as the endpoints for the range of directions around each local maximum. The more confident local maxima, i.e., ones that have a steeper gradient around the local maxima themselves, have a smaller distance between the endpoints. Broad local maxima have a wide range of direction solutions with similar likelihood, with endpoints that are further apart (see Fig. 9). The wind directions associated with each local maximum are saved along with the DIR ranges. The directions associated with the local maxima are used for the nudged field that initializes the ambiguity selection. Our implementation of DIR differs from that in [8] in which a fixed threshold was used, whereas we use a threshold that is varied under certain circumstances.

The DIR-modified ambiguity selection follows the baseline ambiguity selection procedure until an ambiguity is chosen. Once an ambiguity is selected, a new closest-to-median value is chosen from the DIR range of directions associated with the chosen ambiguity. The DIR range is spaced at 1.0° steps. A variety of steps were tested and the 1.0° interval proved to be computationally efficient while providing similar results compared to the finer resolution steps.

The direction within the DIR range closest to the circular median of the local median filter window is chosen to replace the direction for the chosen ambiguity of the center WVC (see Fig. 9). If the difference between the chosen value from between the endpoints is greater than 5° from the current ambiguity direction, the ambiguity choice is updated and the direction for that ambiguity is changed to the value chosen

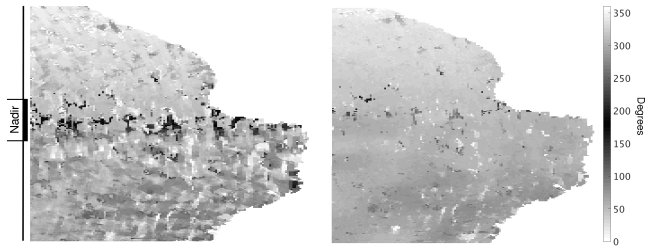


Fig. 10. Images of selected UHR wind directions before and after DIR is applied. The 425×625 km direction field shown includes part of the nadir region of the swath. The white area is land. (Left) Nudged UHR field without a MAS applied. (Right) Same region with the DIR-modified ambiguity selection scheme applied. Colorbar: direction of each location in degrees. Many WVCs with inconsistent directions in the nudged UHR field have the flexibility to become more consistent after DIR is applied.

from between the endpoints; otherwise, the value is not changed. This process, like the baseline MAS, continues until it converges or the maximum number of iterations (200) is reached. Occasionally, the algorithm does not converge but oscillates between sets of values. When the number of changed ambiguities in an iteration remains the same for five iterations in a row, the process is terminated. The number of changed ambiguities when this happens is typically less than 50 out of a swath with thousands of WVCs.

Even when using DIR, nadir WVCs can still have inconsistent ambiguity choices. To ameliorate the inconsistencies, the threshold for nadir WVCs is adjusted to increase the distance of each endpoint from the maxima by 15° on either side. Adjusting the threshold provides additional flexibility in creating consistent fields. Fig. 10 shows how the modified DIR improves the wind estimates in the nadir region, resulting in a more consistent, smoother field.

We note that the DIR threshold can fall below all possible values of the objective function. In the case that endpoints are not found because the threshold does not intersect the objective function, an arbitrary DIR range of $\pm 15^\circ$ from the ambiguity's direction is assigned.

While TN was also developed for, and used in, QuikSCAT processing, we do not use TN in the RapidScat UHR nudging process. TN is designed to improve the accuracy of ambiguity selection in the far swath, which it does by changing the number of ambiguity selection choices when generating the nudged field. Because there are typically fewer ambiguities available in the far swath for RapidScat, TN's limiting the number of ambiguities has little effect on those regions for RapidScat.

V. DEALING WITH WVCs WITH ONLY A SINGLE AMBIGUITY

The limited azimuth diversity, upwind/downwind asymmetry in the nadir region, and noise can result in some WVCs having only a single ambiguity. Approximately 1.6% of all WVCs in a RapidScat swath have only a single ambiguity after the wind retrieval process and greater than 99% of all WVCs with only a single ambiguity are found within 125 km of the nadir track.

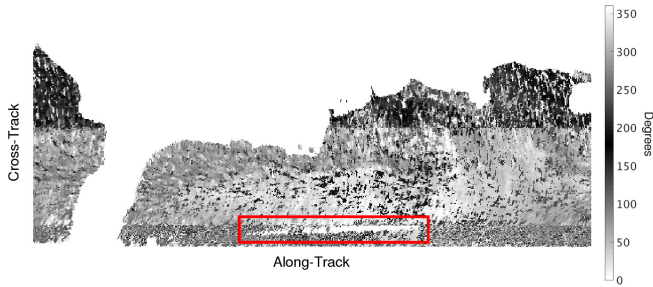


Fig. 11. Direction field of a portion of a swath showing only the first ambiguity choices for all WVCs. The directions on either side of the nadir track are approximately 180° apart. WVCs with only a single ambiguity lie in the areas just on either side of the center dividing lines and are not distinguishable from the ambiguities around them. The long white patch in the boxed region is a data gap resulting from sector blanking.

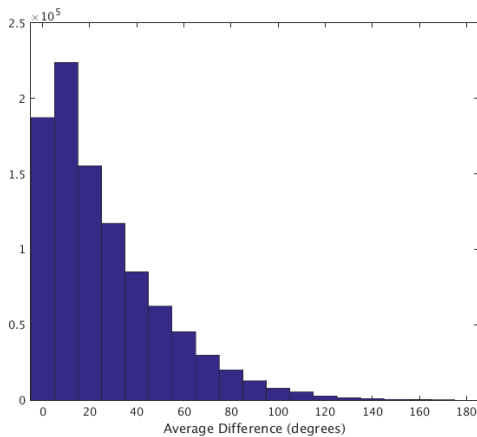


Fig. 12. Histogram of the average difference in direction between WVCs with a single ambiguity and the surrounding first ambiguity choices in a 3×3 WVC window.

Unfortunately, WVCs with only one ambiguity create complications when trying to generate a consistent wind field. WVCs with only one ambiguity have no flexibility to blend in with surrounding WVCs and tend to force the ambiguity selection, but they are often noisy. Even with DIR applied, inconsistencies due to single ambiguity WVCs persist, see Fig. 10 (the dark spots are WVCs with a single ambiguity).

The direction associated with single ambiguity WVCs is often inconsistent with the optimum wind field, though most are consistent with the first ambiguity choices (the ambiguity with the highest likelihood value out of the four) of WVCs surrounding them. This is evident in Fig. 11, which shows a direction field composed of only the first ambiguity choices for each WVC. The nadir track is visible where the angles that are about 180° apart meet.

Fig. 12 shows a histogram of the average difference between the direction of single ambiguity WVCs with the directions of the first ambiguities surrounding it within a 3×3 WVC window. A total of 958 582 WVCs with a single ambiguity are taken from 18 different swaths to create this plot. A majority of the WVCs with a single ambiguity have an average difference less than 50° from the surrounding WVCs. This confirms

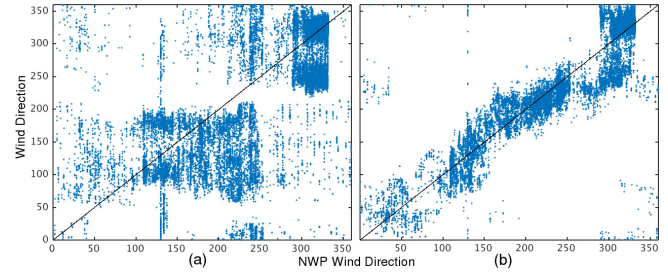


Fig. 13. Scatter plots of wind direction for (a) WVCs with a single ambiguity from one swath plotted against collocated NWP winds and (b) same collocations, but processed with DIR and AA. Note the improved correlation with the NWP winds in (b).

that the directions associated with single ambiguity WVCs are generally consistent with other first ambiguities. However, the first ambiguity is not always the best choice compared to the large-scale wind flow. In this situation, the single ambiguity cases are inconsistent.

To improve the accuracy of WVCs with a single ambiguity, we arbitrarily add two “AAs” to WVCs with only one ambiguity. Analysis of multiple reviews shows that the average number of ambiguities in WVCs surrounding single ambiguity WVCs is two or three.

Experimentally, we find that two AAs set to $\pm 120^\circ$ from the original ambiguity, each with DIR range of $\pm 15^\circ$ and the same wind speed as the single ambiguity provide additional options for the ambiguity selection that result in a reduced error in the single ambiguity areas. We also considered running the ambiguity selection with single ambiguities excluded as well as very large DIR ranges. We consistently found the AA approach to outperform the alternative approaches.

Fig. 13(a) shows WVCs with a single ambiguity from one nudged field swath collocated with NWP winds. Fig. 13(b) shows the same WVCs after AAs are added to the DIR wind retrieval process, note the improved correlation. The result is a much stronger correlation, which is visible by how much closer it follows the $y = x$ line. We conclude that adding AAs to single ambiguity WVCs improves the selected wind direction accuracy. UHR estimates with AAs are further validated in Section VI.

VI. VALIDATION OF NEAR-COASTAL UHR ESTIMATES WITH DIR AND AAS

RapidScat UHR wind estimates with DIR and AAs (hereafter referred to as UHRAA) are validated using the same approach as the UHRB near-coastal validation described in Section II. An analysis of the wind speed accuracy is described in Section VI-A. The results of the wind direction comparison are in Section VI-B.

A. UHRAA Wind Speed Accuracy

In this section, we consider UHRAA wind speed validation. Fig. 14 shows UHRAA and L2B wind speeds plotted against collocated NDBC buoy measurements. As was

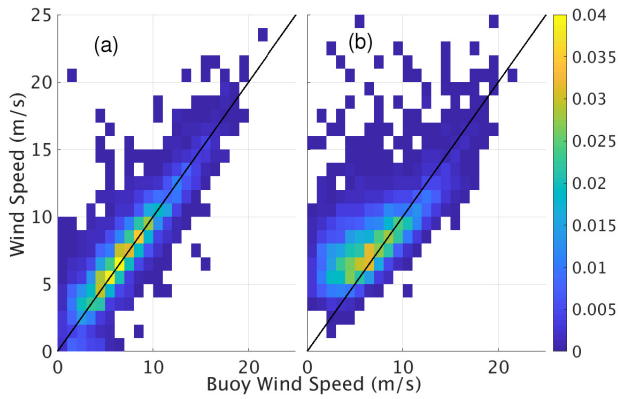


Fig. 14. Scatter density plots of (a) L2B and (b) UHRAA wind speeds plotted against collocated buoy wind speed measurements. The UHRAA estimates have a tighter fit around the $y = x$ line for winds in the range of 5–10 m/s compared to the UHRB estimates, compare Fig. 3.

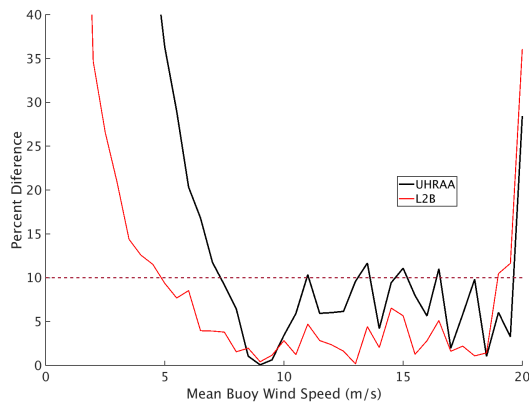


Fig. 15. Percentage difference of mean L2B and mean UHRAA estimates from mean buoy measurements. Horizontal dashed line: 10% difference boundary. For wind speeds greater than 7 m/s, the UHRAA estimates have about twice the error of L2B wind speed estimates.

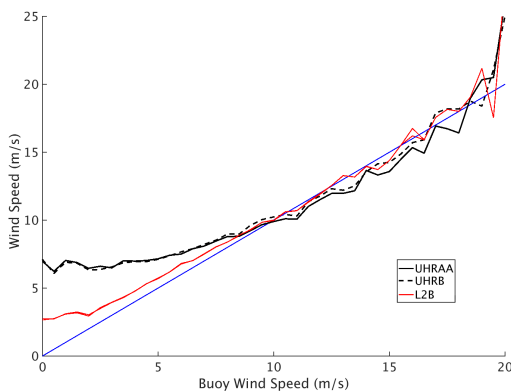


Fig. 16. Mean UHRAA, UHRB, and L2B wind speeds verses collocated mean buoy wind speeds.

done in Section II, the UHRAA estimates are averaged over a 5×5 window to better match the resolution of the lower resolution measurements. The UHRAA estimates are slightly more concentrated around the $y = x$ for estimates between 5 and 10 m/s than the UHRB estimates in Section II. Despite the higher concentration around the $y = x$ line, Fig. 15

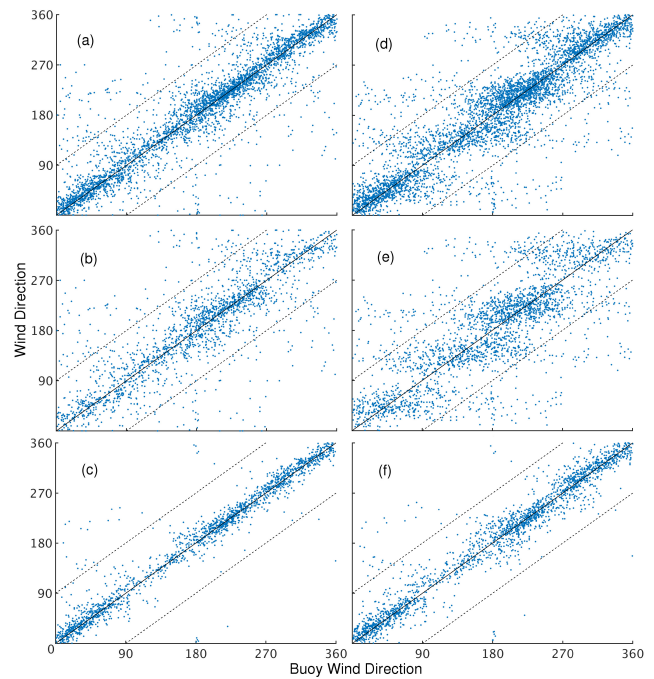


Fig. 17. Scatter plots of (a)–(c) RapidScat L2B and (d)–(f) UHRAA wind directions with collocated buoy measurements sorted by wind speed. (Top row) Collocations at all wind speeds. (Middle row) Collocations with wind speeds below 7 m/s. (Bottom row) Collocations with wind speeds above 7 m/s. Dashed lines: difference of 90° from the ideal $y = x$ line. Due to the circular nature of direction values, for clarity we wrapped the points in the corners $x < 90^\circ, y > 270^\circ$ by subtracting 360° and $x > 270^\circ, y < 90^\circ$ by adding 360° .

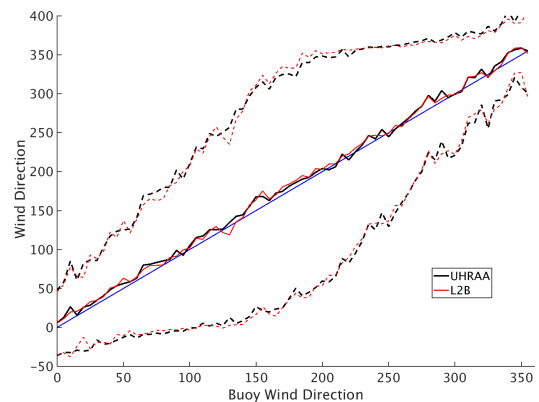


Fig. 18. Plot of the circular means for UHRAA and L2B wind directions collocated with buoy measurements. Included also is a $y = x$ line and a one standard deviation line of the angular difference for both UHRAA and L2B (dashed lines).

shows that, on average, the UHRAA wind speed estimates are slightly higher than the UHRB estimates (compare to Fig. 4). The UHRAA estimates cross the 10% threshold multiple times in the wind speed range from 8 to 20 m/s. Fig. 16 shows UHRAA, UHRB, and L2B mean wind speeds. UHRAA means closely follow UHRB mean values. The similarity between the UHRAA and the UHRB results suggests that the modified UHR ambiguity selection algorithm is choosing the close-to-optimal ambiguities.

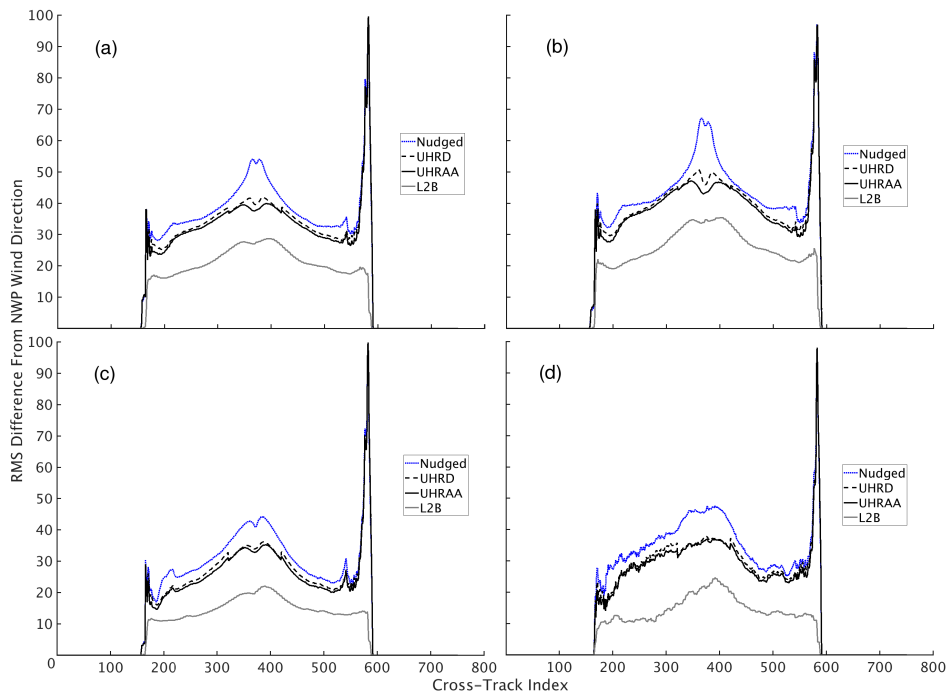


Fig. 19. RMS difference between different versions of UHR wind estimates and NWP sorted by wind speed and plotted against cross-track WVC number. RMS difference between L2B and NWP is also included in each plot. (a) Includes all wind speeds. (b) Wind speeds below 8 m/s. (c) Wind speeds 8–15 m/s. (d) Collocations with wind speeds greater than 15 m/s. Adding the MAS lowers the rms value across the swath for all wind speeds. The addition of AA lowers the rms in the nadir for all wind speeds.

B. UHRAA Wind Direction Accuracy

An analysis of UHRAA wind direction is detailed in this section. Fig. 17 shows UHRAA wind direction estimates collocated with offshore buoy measurements. L2B collocated measurements are plotted again for convenience. The dashed lines in the plot represent a 90° difference from buoy measurements. UHRAA estimates are noisier than the ideal UHRB estimates in Fig. 6, but still match up fairly well with the L2B estimates. Noticeable improvement can be seen for estimates above 7 m/s. At higher wind speeds, the UHRAA estimates are grouped tighter around the $y = x$ line than UHRB direction estimates. For wind speeds below 7 m/s, the UHRAA estimates appear more spread out than UHRB estimates.

Fig. 18 shows the mean directions of UHRAA and L2B estimates binned at 5° . Both the UHRAA and L2B mean lines closely follow the $y = x$ line. Like UHRB estimates, the UHRAA standard deviation line of the difference closely follows the L2B standard deviation line. Fig. 19 shows the rms difference between different versions of UHR wind direction estimates and L2B wind direction estimates compared to NWP winds. The plot includes rms values for a month's worth of L2B, UHR nudged, UHRD (UHR with DIR but without AAs) and UHRAA estimates. UHRD decreases the rms difference across the swath, especially in the nadir region. UHRAA further decreases in rms in the nadir region even more. The rms across the swath for all wind speeds is decreased by the algorithm improvements. A visual inspection also confirms these results. Fig. 20 shows a section of L2B, UHR nudged, and UHRAA processed winds along the East Coast of the

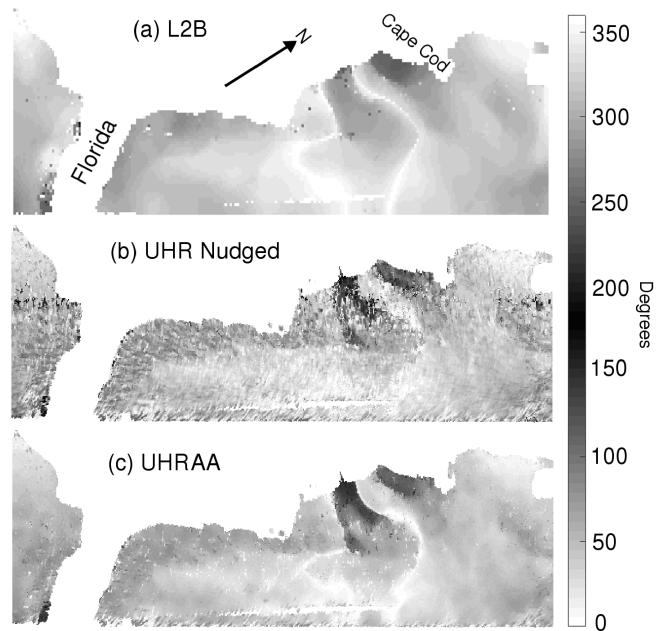


Fig. 20. Comparison of estimated RapidScat wind directions for various algorithms. (a) L2B, (b) UHR nudged, and (c) UHRAA wind direction fields. The swaths are $1877.5 \text{ km} \times 2777.5 \text{ km}$ on the East Coast of the United States, see text.

United States. The UHR nudged field is noisier than the L2B and some of the wind features are difficult to distinguish. UHRAA reduces the noise in the nudged field while preserving the L2B wind features at a higher resolution.

VII. CONCLUSION

UHR winds provide finer spatial resolution than L2B winds at the expense of higher noise levels. In this paper, we have implemented improvements in UHR wind retrieval and ambiguity selection. We conclude that while the improved UHRAA wind estimates are noisier than L2B wind estimates, on average they match up well with L2B estimates. UHRAA wind direction estimates are comparable with L2B wind direction estimates, especially at wind speeds above 7 m/s. UHRAA wind direction estimates also produce more spatially consistent wind direction fields than conventional pointwise UHR nudged wind direction estimates, as seen in the example swaths in Fig. 20.

UHRAA wind speed estimates have similar performance compared to L2B wind speed estimates. However, at low wind speeds, UHRAA wind speed estimates are biased higher than L2B estimates. This is due to lower SNR at low wind speeds and the higher noise level at the finer resolution. The higher bias is an expected result of the higher noise level [18].

The results of the UHRAA are similar to or better than the optimal UHRB case described in Section II. The similarity means that the new wind retrieval algorithm is selecting nearly optimal values. The results show that the changes to processing improve UHR wind retrieval in near-coastal regions.

REFERENCES

- [1] F. T. Ulaby and D. G. Long, *Microwave Radar and Radiometric Remote Sensing*. Ann Arbor, MI, USA: Univ. Michigan Press, 2014.
- [2] P. S. Chang *et al.*, "Operational use and impact of satellite remotely sensed ocean surface vector winds in the marine warning and forecasting environment," *Oceanography*, vol. 22, no. 2, pp. 194–207, Jun. 2009.
- [3] S. L. Durden and D. Perkovic-Martin, "The RapidScat ocean winds scatterometer: A radar system engineering perspective," *IEEE Trans. Geosci. Remote Sens.*, vol. 5, no. 3, pp. 36–41, Sep. 2017.
- [4] Physical oceanography distributed active archive center (PO.DAAC), "SeaWinds's user guide," vol. 3, Jet Propulsion Laboratory internal document D-18053, Jun. 2006.
- [5] J. Yang and J. Zhang, "Evaluation of ISS-RapidScat wind vectors using buoys and ASCAT data," *Remote Sens.*, vol. 10, no. 4, p. 648, 2018.
- [6] N. Ebuchi, "Evaluation of marine vector winds observed by rapidscat on the international space station using statistical distribution," in *Proc. IEEE Int. Geosci. Remote Sens. Symp. (IGARSS)*, Jul. 2015, pp. 4901–4904.
- [7] W. T. Liu and W. Tang, "Equivalent neutral wind," Jet Propuls. Lab., Pasadena, CA, USA, Tech. Rep. NASA-CR-203424, 1996.
- [8] B. W. Stiles, B. D. Pollard, and R. S. Dunbar, "Direction interval retrieval with thresholded nudging: A method for improving the accuracy of QuikSCAT winds," *IEEE Trans. Geosci. Remote Sens.*, vol. 40, no. 1, pp. 79–89, Jan. 2002.
- [9] F. M. Naderi, M. H. Freilich, and D. G. Long, "Spaceborne radar measurement of wind velocity over the ocean—an overview of the NSCAT scatterometer system," *Proc. IEEE*, vol. 79, no. 6, pp. 850–866, Jun. 1991.
- [10] S. J. Shaffer, R. S. Dunbar, S. V. Hsiao, and D. G. Long, "A median-filter-based ambiguity removal algorithm for NSCAT," *IEEE Trans. Geosci. Remote Sens.*, vol. 29, no. 1, pp. 167–174, Jan. 1991.
- [11] H. Schultz, "A circular median filter approach for resolving directional ambiguities in wind fields retrieved from spaceborne scatterometer data," *J. Geophys. Res.*, vol. 95, no. C4, pp. 5291–5303, 1990.
- [12] R. D. Lindsley, "Enhanced-resolution processing and applications of the ASCAT scatterometer," Ph.D. dissertation, Dept. Elect. Comput. Eng., Brigham Young Univ., Provo, UT, USA, 2015.
- [13] M. W. Spencer, W.-T. Tsai, and D. G. Long, "High-resolution measurements with a spaceborne pencil-beam scatterometer using combined range/Doppler discrimination techniques," *IEEE Trans. Geosci. Remote Sens.*, vol. 41, no. 3, pp. 567–581, Mar. 2003.
- [14] B. A. Williams and D. G. Long, "A reconstruction approach to scatterometer wind vector field retrieval," *IEEE Trans. Geosci. Remote Sens.*, vol. 49, no. 6, pp. 1850–1864, Jun. 2011.
- [15] B. A. Williams, M. P. Owen, and D. G. Long, "The ultra high resolution QuikSCAT product," in *Proc. IEEE Radar Conf.*, May 2009, pp. 1–6.
- [16] A. M. Plagge, D. C. Vandemark, and D. G. Long, "Coastal validation of ultra-high resolution wind vector retrieval from QuikSCAT in the gulf of maine," *IEEE Geosci. Remote Sens. Lett.*, vol. 6, no. 3, pp. 413–417, Jul. 2009.
- [17] *National Data Buoy Center*. Accessed: Apr. 2, 2018. [Online]. Available: <http://www.ndbc.noaa.gov>
- [18] M. H. Freilich and R. S. Dunbar, "The accuracy of the NSCAT 1 vector winds: Comparisons with National Data Buoy Center buoys," *J. Geophys. Res.*, vol. 104, no. C5, pp. 11231–11246, 1999.
- [19] J. C. Russ, *The Image Processing Handbook*. Boca Raton, FL, USA: CRC Press, 1995.



Nolan Hutchings received the B.S. degree in electrical engineering from Brigham Young University (BYU), Provo, UT, USA, in 2017, where he is currently pursuing the master's degree in electrical engineering.

Since 2016, he has been with the Microwave Earth Remote Sensing Laboratory, BYU, where he has been involved in ultrahigh-resolution scatterometry.



David G. Long (S'80–SM'98–F'08) received the Ph.D. degree in electrical engineering from the University of Southern California, Los Angeles, CA, USA, in 1989.

From 1983 to 1990, he was with the NASA Jet Propulsion Laboratory (JPL), Pasadena, CA, USA, where he developed advanced radar remote sensing systems. From 1996 to 1997, he was the Project Engineer on the NASA Scatterometer (NSCAT) Project with JPL. He also managed the SCANSAT Project, the precursor to SeaWinds, which was flown in 1999 on QuikSCAT, in 2002 on ADEOS-II, and in 2014 on the International Space Station. He is currently a Professor with the Electrical and Computer Engineering Department, Brigham Young University (BYU), Provo, UT, USA, where he teaches upper division and graduate courses in communications, microwave remote sensing, radar, and signal processing and also the Director of the Center for Remote Sensing, BYU. He is also the Principal Investigator on several NASA-sponsored research projects in remote sensing. He has authored or co-authored over 400 publications in various areas including signal processing, radar scatterometry, and synthetic aperture radar. His research interests include microwave remote sensing, radar theory, space-based sensing, estimation theory, signal processing, and mesoscale atmospheric dynamics.

Dr. Long was a recipient of the NASA Certificate of Recognition several times and is an Associate Editor for IEEE GEOSCIENCE AND REMOTE SENSING LETTERS.